文章编号：1001-9014(2021)05-0627-07

DOI：10. 11972/j. issn. 1001-9014. 2021. 05. 008

Analysis of oscillation-starting characteristics in millimeter wave extended interaction oscillators

XU Che, MENG Lin, YIN Yong*, BI Liang-Jie, CHANG Zhi-Wei, LI Hai-Long, WANG Bin

(School of Electronic Science and Engineering, University of Electronic Science and Technology of China Chengdu 610054, , China)

Abstract: The investigations of the oscillation-starting characteristics of a ladder-type RF circuit are proposed to overcome the limitation of high ohmic loss for development of millimeter-wave extended interaction oscillators (EIOs). Based on PIC-simulations, quantitative calculations and theoretical analyses, the designed and fabricated W-band EIO is proved to have the possibility of greatly reducing the oscillation-starting current. By optimizing five aspects including the gap number, cavity dimension, field distribution, operation voltage, and surface loss, the oscillation-starting current of the EIO can be reduced to 0. 43 A with a beam voltage of 17. 5 kV. According to cold test experiment, the output power attenuation is analyzed and predicted.

Key words: extended interaction oscillator, oscillation-starting condition, slow wave structure, vacuum electronics

毫米波扩展互作用振荡器的起振特性研究

徐 彻, 蒙 林, 殷 勇*, 毕亮杰, 常志伟, 李海龙, 王 彬

(电子科技大学 电子科学与工程学院,四川 成都 610054)

摘要:为克服高欧姆损耗对发展毫米波频率的扩展互作用振荡器(EIO)的限制,本文开展了对于阶梯型射频电路的振荡起始特性研究。通过PIC仿真模拟、定量计算和理论分析,本文证明了一个被设计和制作的W波段EIO具有大幅度降低振荡启动电流的可能性。通过对间隙数、腔体尺寸、场分布、工作电压和表面损耗五个方面的优化,在电子注电压为17.5kV时,该EIO的振荡起始电流可降至0.43A。根据冷测实验结果,本文还对输出功率衰减进行了分析和预测。

关 键 词:扩展互作用振荡器;起振条件;慢波结构;真空电子学

中图分类号:TN129　　**文献标识码**:A

Introduction

Millimeter wave extended interaction devices (EIDs), including extended interaction oscillators (EIOs) and extended interaction klystron amplifiers (EIKAs), are attractive for many applications because of the requirement in the fields of plasma diagnosis, material science, spectroscopy and commerce [1-3]. EID uses the rectangular ladder-type resonant slow wave structure (SWS) as beam wave interaction, which has the characteristics of both slow wave structure and resonant cavity. Thus, EIDs have great advantages in miniaturization, high frequency and high-power generation [4-11]. At present, the products of EIOs manufactured by Communications & Power Industries can commercially reach several kilowatts to tens of kilowatts in the millimeter wave band, while the output power in the THz band is only several watts to tens of watts. [12, 13].

The high power and high efficiency EIO is so attractive that it is widely studied because it can provide more efficient beam-wave interaction (this can be embodied by the relatively large value of *R/Q*) while ensuring the same

Received date: 2020- 09- 03, **revised date**: 2021- 07- 08　　**收稿日期**:2020- 09- 03,**修回日期**:2021- 07- 08

Foundation items: Supported by the National Natural Science foundation of China (61671116, 61771096, 11905026), National Key Research and Development Program of China (2019YFA0210202) and Fundamental Research Funds for the Central Universities (ZYGX2019Z006, ZYGX2019J012)

Biography: XU Che (1992-), male, Chengdu, China, Ph. D. Research area involves millimeter and terahertz vacuum electronic devices. E-mail: chexu1992@163. com

* **Corresponding author**: E-mail: yinyong@uestc. edu. cn

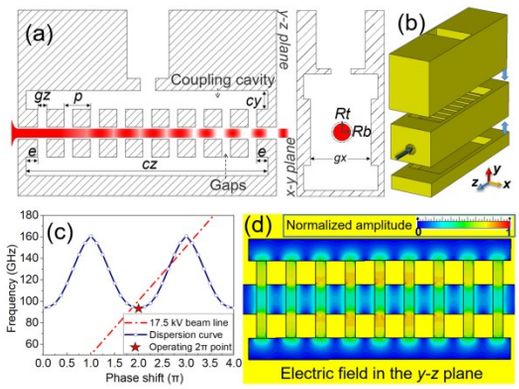

Fig. 1 (a), (b) Layout of the EIO circuit. (c) Dispersion diagram of the EIO and (d) the electric distribution of the operation 2π mode.
图1 (a), (b) EIO电路的结构布局。(c) 该EIO的色散曲线图。(d) 2π模式的电场分布图

current density as the conventional klystron oscillators. Since its electric field coupling form is similar to a TE_{10} wave which is transmitted to the coupling cavity through a rectangular gap [10], the frequency of EIO mainly depends on the gap structure parameters. In other words, the cutoff frequency of 2π mode is determined by *gx*, as shown in Fig. 1. At millimeter and sub-millimeter wave band, the achievable output power of the conventional O-type vacuum electronic devices (VEDs), including EIDs, is greatly limited by the beam current and voltage across the devices. At this stage, with the intensification of the research on high frequency up to THz band, the surface current loss of the device has increased significantly along with the sharp decline in skin depth. Under such circumstance, the threshold of EID oscillation starting condition is further raised. Therefore, based on a certain cathode current, a lower oscillation-starting threshold is required for developing higher frequency EIDs.

With its inherent characteristics of high coupling impedance *R/Q* [4, 14], high-frequency EIO provides favorable conditions for obtaining lower oscillation start-up conditions among VEDs. In this paper, we analyzed the oscillation start-up characteristics of a W-band EIO based on CST Microwave Studio [15] simulations and cold test experiments. Firstly, the structural composition, high-frequency and dispersion characteristics of the specific-designed W-band EIO are introduced. Secondly, based on the small signal theory, the quantitative study of starting current in a millimeter wave EIO is introduced. In this aspect, the accuracy of oscillation-starting current is validated by both PIC-simulation codes and the quantitative calculations (in Sec. III). Thirdly, based on the influences of five factors (Influences of gap number, cavity dimension, field distribution, operation voltage, and surface loss) related to the initial conditions of oscillation-starting directly, the circuit oscillation start-up principle is studied analytically and simulatively. Particularly, the oscillation start-up analyses of high-frequency characteristics provide a feasible method to directly overcome the limitations of high ohmic loss and high start-up standards in high-frequency band and even terahertz.

1 Description of the designed EIO circuit

The structure of the designed EIO circuit, as shown in Fig. 1(a), mainly consists of nine ladder-like interaction gaps, one 0.7 mm-diameter beam tunnel and two 2.20*0.50*6.74 mm coupling cavities distributed on both sides of the SWS. The period *p* of 0.76 mm determines the electron transit velocity, which is directly related to the operation voltage. The gap dimensions *gx* and *gz* are 1.8 mm and 0.26 mm respectively. For manufacturing requirements, the SWS can be split into three parts across the *x*–*z* plane on both sides of the coupling gaps (Fig. 1(b)). The UV-LIGA technique [16] or Nano-CNC machining technology [17] can be used to fabricate each part.

Among O-type devices, the operating mode of the rectangular resonator cavity is TM mode. In high frequency band, over-mode structures have received increasing attention, because they can reduce the machining difficulty and increase the power capacity. However, they also inevitably weaken the beam-wave interaction because of the smaller coupling coefficient *M* and the coupling impedance *R/Q* [18, 19]. The *R/Q* can be expressed as

$$\frac{R}{Q}=\frac{\left(\int_a^b E_z dl\right)^2}{2wW_s}, \tag{1}$$

which is a measure of the E_z field acting on the electrons for a given total stored energy (W_s) and angular frequency (w).

Here, we choose the fundamental TM_{110}-like mode scheme as the research object to take advantage of its superior high frequency characteristics in the aspect of oscillation starting. The dispersion curve and electric field distribution of the fundamental 2π mode are shown in Fig. 1(c) and Fig. 1(d), respectively. As shown in Fig. 1(c), the beam voltage should be slightly higher than the 2π operating point to meet the synchronization condition of EIO, which is that electron velocity v_e is slightly greater than phase velocity v_p. When the EIO works in the 2π mode, the electric field with periodic standing wave distribution (Fig. 1(d)) can effectively modulate the electron beam.

2 Oscillation-starting condition and high frequency characteristics

A distinguishing and important feature of an oscillator is that there exists a definite minimum electron beam current value, below which the resonant cavity will not oscillate. When considering the beam loading in the circuit, the normalized beam-loading conductance g_e (or the beam-loading conductance G_e) is the key factor to discuss the oscillation or amplification. The g_e satisfies the resonance condition only when the value is negative. In this state, the energy exchange between the electron beam and the electric field makes the electron energy flow to the circuit, thus establishing the stable electric

field. Based on the one-dimensional linear theory, the starting current (I_{st}) [20, 21] of EID cavity can be derived from:

$$I_{st} = \frac{aU}{\frac{R}{Q}Q_l(-g_e)_{\max}}, \tag{2}$$

The parameter U is the operation voltage. The a of 0.5 is the empirical correction factor, which is related to the operation frequency and surface roughness. According to the small signal theory of klystron, the general derivation of small signal normalized beam-loading conductance g_e with space-charge is given by [21]:

$$g_e = \frac{G_e}{G_0} = \frac{G_0\beta_e}{4}\left[\frac{M^2(\beta_e+\beta_q)-M^2(\beta_e-\beta_q)}{2\beta_q}\right], \tag{3}$$

where the G_0 stands for the DC beam conductance, I_0/U_0. The $\beta_e=\omega/v_e$ and $\beta_q=\omega_q/v_e$ are the propagation constants of the DC beam and reduced plasma respectively. The ω is the RF radian frequency, the ω_q is the reduced-plasma angular frequency and v_e is the DC beam velocity. The coupling coefficient M can be obtained by:

$$M(\beta_e) = \frac{\int_{-\infty}^{+\infty} E(z)\exp(-j\beta_e z)dz}{\int_{-\infty}^{+\infty}|E(z)|dz}. \tag{4}$$

the loaded quality factor Q_l can be obtained from:

$$\frac{1}{Q_l} = \frac{1}{Q_0} + \frac{1}{Q_e} + \frac{1}{Q_b}. \tag{5}$$

The Q_0 and Q_e are inherent quality factor and external quality factor, respectively. Where Q_b is the beam-loaded quality factor [21], which can be determined by the equation:

$$\frac{1}{Q_b} = G_e\left(\frac{R}{Q}\right). \tag{6}$$

Generally, the oscillation-starting condition of an EIO circuit is determined by many factors such as the structural parameters, beam voltage U, and the electromagnetic field distribution. These factors collectively affect the resonant starting condition and can be characterized by the I_{st}, which can be derived from Eq. (2).

2.1 Influences of the gap number N_g on the oscillation characteristics

Among the structural parameters, the number of gaps N_g in the EIO structure should be considered first. The N_g plays a direct effect on the interaction ability of EIDs. As shown in Fig. 2(a) and Fig. 2(b), in quantitative analysis, it affects the values of M^2R/Q and normalized beam-loading conductance g_e. Fig. 2(a) shows the curve of M^2R/Q with voltage in the cases of 5-11 gaps. It can be concluded that the increase of N_g will enlarge the values of M^2R/Q and negative-maximum g_e. While the corresponding abscissa voltage value will change inevitably. The characteristic parameters of this EIO, such as inherent quality factor Q_0, external quality factor Q_e, R/Q, M^2R/Q and frequency separation Δf, change with the number of gaps as shown in Table 1. Among these parameters, the increasement of N_g can most effectively raise the value of R/Q. The energy exchange of beam-wave interaction is proportional to R/Q. An EIO cavity possess the shorted slow-wave structure terminal, which has superior in enlarging the value of R/Q [14]. However, the upper limit of N_g does exist: Firstly, when the number of gaps increases, the length of the circuit will become longer, which may cause the over-bunching effect [20]. In this case, a part of electrons regain energy from the electric field at the end of the circuit, thus reducing the interaction efficiency. Secondly, in the condition of over-amount gap number, the sudden decrease of the frequency interval Δf between adjacent modes makes it easier for the competing modes to be excited. In conclusion, an extended interaction cavity should not have too small frequency separation nor undersized R/Q. As a result of the tradeoff between the interaction ability and mode-competition of the structure, the nine-gap EIO structure is the most appropriate. In addition, in order to obtain the min-

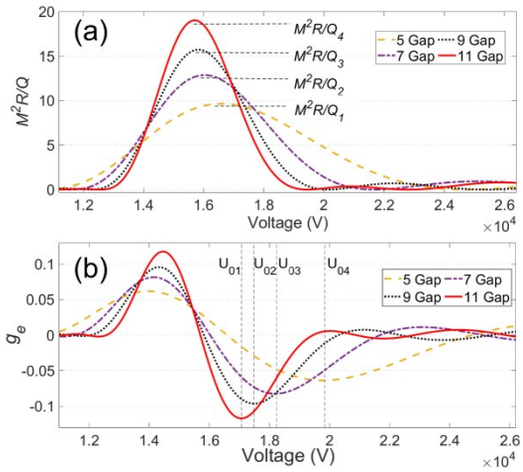

Fig. 2 The (a) M^2R/Q and the (b) normalized beam-loading conductance variations with the beam voltage in the cases of 5-11gaps.
图2 在5-11间隙的情况下,(a) M2R/Q 和 (b) 归一化电子注负载电导随电子注电压的变化

Table 1 Characteristics of the operation mode with different gap number
表 1 在不同间隙数情况下的特性参数

Model	Gap Number (N_g)	Q_0	Q_e	R/Q (Ω)	U_0	$M^2R/Q_{\max}$ (Ω)	f-2π (GHz)	f-2π+1 (GHz)	Δf (GHz)
1	5	808.54	491.04	311.44	19.79	9.65	93.44	97.70	4.26
2	7	811.88	389.48	435.14	18.21	12.87	93.43	95.64	2.21
3	9	811.22	822.85	542.86	17.50	15.73	93.53	94.87	1.34
4	11	811.24	462.81	667.36	17.07	19.03	93.49	94.50	1.01

imum start-up current, the beam voltage of 17.5 kV corresponding to the maximum value of $-g_e$ was adopted (which derives from Fig. 2(b) and Eq. (3)).

2.2 Influences of the cavity structure on the oscillation characteristics

Table 2 Circuit characteristic parameters versus cavity height

表 2 电路特性随耦合腔高度的变化

Model	cy(mm)	R/Q	Q_l	$-g_e$	I_{stt}(A)	I_{sts}(A)
1	0.4	548.58	230.51	0.077	0.90	0.70
2	0.5	541.86	407.87	0.096	0.41	0.43
3	0.6	512.15	273.78	0.087	0.72	0.80

An important feature of the extended interaction oscillator is the coupling cavity distributed on both sides of the periodic grating, which determines the frequency selection and affects various cavity characteristics. Among the parameters, the cavity height cy plays a decisive role in the circuit characteristics of the EIO. Fig. 3(a) shows the operating frequency, oscillation-starting time T_s and radiation power versus the vertical dimension of the coupling cavity cy. As an electron beam of 17.5 kV and 0.8 A is injected, the output power P_{out} of up to 908 W and a -3dB mechanical width of 0.40-0.53 mm was observed. There is a sharp decline of the P_{out} beyond the -3dB mechanical width, which is caused by the change of circuit characteristic parameters.

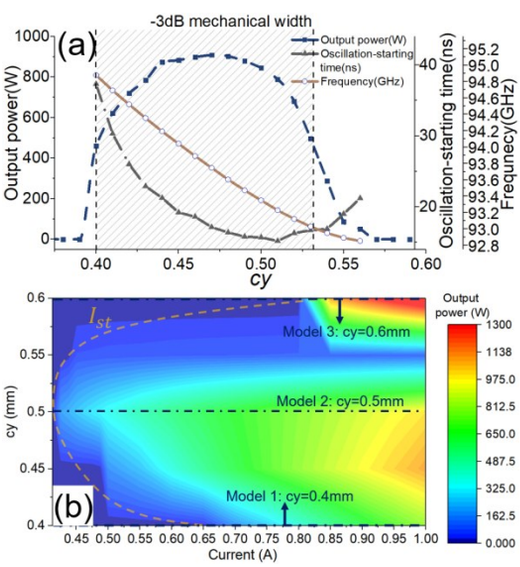

Fig. 3 (a) Output radiation power, operating frequencies, and oscillation-starting time versus cy. (b) Three-dimensional PIC simulation results: the 2D variation of output power relative to cy and the emission current.

图 3 (a) 输出辐射功率、工作频率和振荡开始时间与cy的关系。(b) 三维的PIC模拟结果:输出功率随cy和发射电流的二维变化

When studying the initial state of oscillation characteristics, the traditional one-dimensional parameter-sweep is not enough to fully reflect the influence of characteristic parameters on the output characteristics. In order to observe the influence of cavity structure on the oscillation-starting conditions, the 2D variation of output power relative to cy and the emission current was calculated more than 100 times, as shown in Fig. 3(b). It can be found from Fig. 3(b) that the I_{st} of the EIO (which is 0.42 A) is relatively low at a cy of 0.5 mm. When the value of cy deviates from 0.5 mm, the I_{st} shows a parabolic-like increase trend. Generally, when the simulated oscillation starting current (I_{sts}) is relatively low, the beam-wave energy transfer efficiency is relatively high, but a low starting current does not equal to high efficiency absolutely. For comparing with the theoretical value, we take three typical cy models with different values of cy. According to simulation and calculation results, their corresponding R/Q, loaded quality factor Q_l, $-g_e$, and theoretical starting current (I_{stt}) values are shown in Table 2. Compared with the Model 1 and 3 in Table 2, the Model 2 has higher Q_l, which means it has stronger frequency selectivity and higher cavity energy storage, and also can provides favorable conditions to achieve the initial state of oscillation. In Table 2, the theoretical I_{stt} obtained by Eq. (2) is basically consistent with the PIC-simulation value I_{sts}. Besides, compared with the Model 1 and 3, the Model 2 has the lower theoretical I_{stt}, which agrees well with the simulation trend in Fig. 3(b).

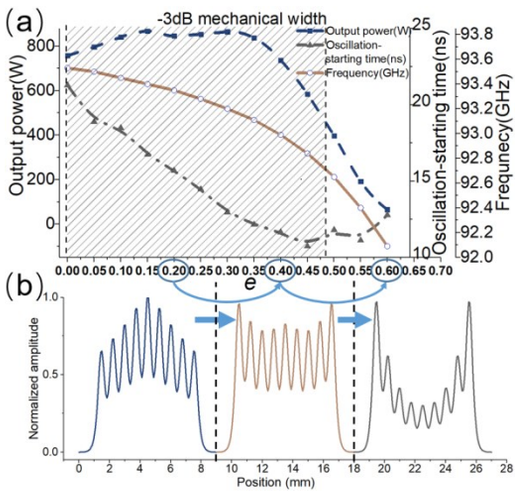

Fig. 4 (a) Output radiation power, operating frequencies, and oscillation-starting time versus e. (b) The distributions of Ez field along the center line of the beam tunnel with the increase of e.

图 4 (a) 输出辐射功率、工作频率和振荡起始时间与e的关系 (b) 随着e的增加,z向电场沿电子注通道中心线的分布

Table 3 Characteristics of the different cavity dimensions on z-zxis

表 3 耦合腔z方向长度变化时的电路特性参数

Model	e (mm)	cz (mm)	R/Q (Ω)	Q_0
1	0.2	6.74	542.86	811.22
2	0.4	7.14	563.28	796.25
3	0.6	7.54	441.30	786.65

2.3 Influences of field distribution on the oscilla-

tion characteristics

The electric field distribution of the 2π mode in the EIO mainly depends on the length of the extended section *e* of the coupling cavity [22]. Fig. 4(a) shows the relationship between the output characteristics and *e* when a cylindrical electron beam with 17.5 kV and 0.8 A is injected. When *e* is less than 0.4 mm, the output power is maintained around 800W, as shown in the Fig. 4(a). However, when *e* is greater than 0.4 mm, there is a sharp decline in output power and frequency, which will negatively affect the output characteristics of the EIO. We found that in the aspects of the coupling strength and output characteristics, there is an associate relationship between the field structure and the output structure. As shown in Fig. 4(b), as *e* increases, the axial electric field of the structure has a suppressing effect from the middle to both sides. As shown in Fig. 1 previously, owing to the output structure of the EIO which is located above the middle of the coupling cavity, the mismatched electric field distribution will suppress the field coupling.

This mismatch is manifested in the decline of the values of *R/Q* and Q_0, as shown in the Table. 3. Therefore, the distribution of electric field should accord with the coupling of output structure. Based on the previous analysis, the *e* of this EIO was determined to be 0.2 mm.

2.4 Influences of operation voltage on the oscillation characteristics

Table 4 Characteristics of the different operating voltage
表 4 不同工作电压下的电路特性参数

Model	*U* (kV)	$-g_e$	I_{stt} (A)	I_{sts} (A)
1	17.5	0.096	0.41	0.42
2	18.0	0.087	0.47	0.52
3	18.4	0.077	0.54	0.70

According to Eq. (2), the operation voltage *U* has a linear correlation with the starting current. However, in the process of voltage variation, the $-g_e$ and *R/Q* will also change accordingly as shown in Fig. 2 previously. Therefore, the design selection of operating voltage will have a direct impact on determining the oscillation start-up conditions.

In this section, three emission models (in Table. 4) with different voltages are simulated and calculated. As the voltage increases, the voltage line in the dispersion curve in Fig. 2(c) will gradually deviate from the 2π mode point, which is conducive to the bunching effect of the electron beam, and the electron efficiency will increase accordingly. Fig. 5 shows the output characteristics of the EIO circuit at 17.5, 18.0, 18.4 kV. When the electron beam current is 0.8 A, their output power are 786 W, 934 W and 1100 W, respectively. However, in addition to the increased electronic energy conversion efficiency, the increased *U* makes the I_{st} of the circuit have an increasing trend, and the parameters are shown in Table 4. This trend is mainly embodied in the variation of the $-g_e$. When the g_e is negative, the slow wave phase velocity is lower than the electron beam

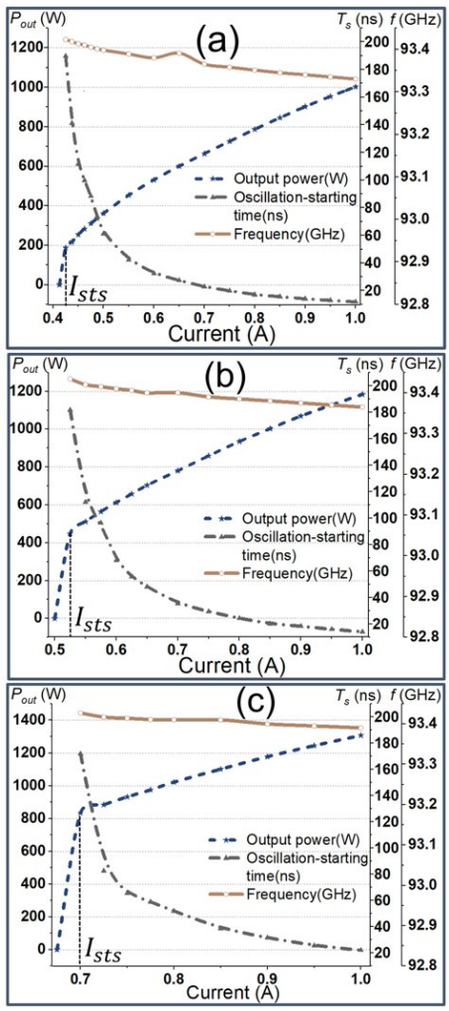

Fig. 5 The circuit output characteristics versus operation current when U is (a) 17.5, (b) 18.0 and (c) 18.4 kV respectively. The oscillation-starting condition is characterized by comparing the output power P_{out}, starting time T_s and operation frequency *f* of the EIO circuit.
图 5 当U分别为(a) 17.5、(b) 18.0和(c) 18.4kV时,电路输出特性与工作电流的关系。通过比较EIO电路的输出功率Pout、启动时间Ts和工作频率f来表征振荡启动条件。

phase velocity, and the beam wave interaction causes the electron beam energy to flow into the electric field. For high frequency extended interaction structures, a relatively high absolute value of g_e is beneficial to reduce the starting current. Accordingly, the Model 1 in Table. 4 has lower oscillation-starting threshold than the Model 2 and 3. In Table 4, the theoretical value I_{stt} and the simulated value I_{sts} show a consistent increasing trend. Therefore, in terms of voltage selection, the rules of high efficiency and low start-up current cannot be followed at the same time. The trade-off between them is essential. In order to facilitate the oscillation-starting of the circuit, the emission model with an operation voltage of 17.5 kV is adopted.

2.5 Discussion of surface loss and fabrication

Due to the influence of surface roughness and impurity doping, the *S*-parameters obtained in the cold measurement experiment usually do not fully conform to the

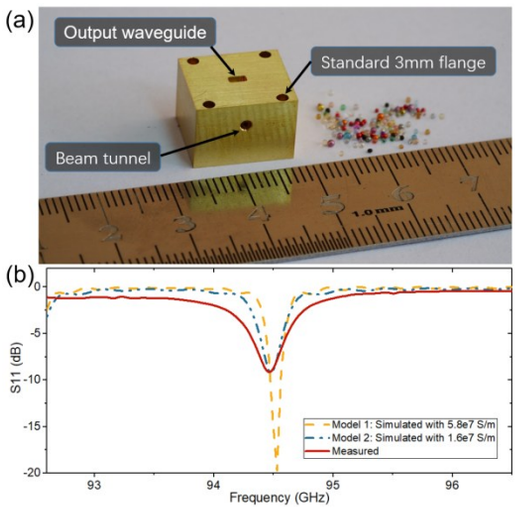

Fig. 6 (a) The fabricated copper EIO structure. (b) Measured values of reflection parameter S11 and simulated values at conductivities of 1.6e7 S/m and 5.8e7 S/m.
图 6 (a) 制作的铜质EIO结构。(b) 在电导率为1.6e7S/m和5.8e7S/m时反射系数S11的实测值和模拟值。

simulation results. Among VEDs, this inconsistency can be represented by the decrease of conductivity [22, 23]. Fig. 6 shows the fabricated EIO circuit and the cold measured reflection coefficient S_{11}. The input-output waveguide and a vector network analyzer are connected by standard 3mm flange to obtain the S_{11}. The amplitude and frequency of the S_{11} coefficient measured in the cold test experiment are -9.13 dB and 94.47 GHz, respectively, which are attenuated compared with -19.71 dB and 94.53GHz in the simulation (Model 1, Fig. 6(b)). When the conductivity decreases to 1.6×10^7 S/m, the frequency and amplitude of S_{11} in experiments and simulations are basically consistent. It can be concluded from the Fig. 6 (b) that there is an additional ohmic loss caused by the surface roughness in the fabricated EIO circuit, which can accordingly reduce the power capacity and radiation power of the circuit. From the experimental monitored S_{11}, the measured value of Q_l is 346.50, which can be derived from

$$Q_l = \frac{f_0}{2\Delta f_b}. \tag{7}$$

Compared with the simulated Q_l of 407.87, this attenuation can be embodied in the increased correction factor a. Where the $2\Delta f_b$ is the -3 dB bandwidth of the measured S_{11}.

Correspondingly, the output characteristics of the circuit with the change of conductivity are simulated, as shown in Fig. 7. The reduction in S_{11} shown previously in Fig. 6(b) is essentially a reduction in power capacity. Therefore, the deviation between the cold-test result and the simulation result can be used to correct the simulation results and make predictions for the hot-test experiments. Then as shown in Fig. 7, the output power in the PIC simulation has also been reduced from 859 W to 471 W. From the above analysis, the accuracy of fabrication also has a significant impact on the oscillation start-up condition, and the weakened electric field may not be sufficient to achieve the condition.

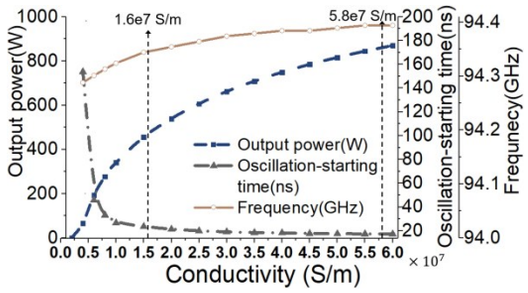

Fig. 7 Output radiation power, operating frequencies, and oscillation-starting time versus conductivity.
图 7 输出辐射功率、工作频率和振荡开始时间与电导率的关系。

3 Conclusion

In summary, the oscillation-starting characteristics of a W-band EIO are analyzed theoretically and experimentally (cold test). Firstly, this paper expounds the starting characteristics of EIO circuit by analyzing the relationship between mode, dispersion, and high frequency characteristics. Secondly, the influences of structural parameters, field distribution, operation voltage, and ohmic loss on the oscillation-starting condition are analyzed through the high frequency characteristic parameters of the circuit. Thirdly, based on the small signal theory, the accuracy of oscillation-starting current is validated by both simulation and cold-test measurement.

This will provide an effective reference for the further research on the oscillation-starting condition of the high-power and high-efficiency EIKs at high frequency band and even terahertz. Further demonstration is ongoing and we plan to reduce the threshold of oscillation initiation by reducing losses to meet the low current hot test experiments.

References

[1] ROITMAN A, BERRY D, STEER B. State-of-the-Art W-Band Extended Interaction Klystron for the CloudSat Program [J]. *IEEE* Trans Electron Devices, 2005, **52**(5): 895-8.
[2] BERRY D, HOROYSKI P, HYTTINEN M, *et al*. Extended interaction klystrons for submillimeter applications; proceedings of the 30th International Conference on Infrared and Millimeter Waves, F, 2005 [C].
[3] WANG Z C, SHANG X W, CAO L L, *et al*. Investigation on a W-band high efficiency extended interaction oscillator based on phase re-synchronization technology [J]. *Journal of Infrared and Millimeter Waves*, 2020, **39**(2): 211-20.
[4] YIN Y, HE W, ZHANG L, *et al*. Simulation and Experiments of a W-Band Extended Interaction Oscillator Based on a Pseudospark-Sourced Electron Beam [J]. *IEEE* Trans Electron Devices, 2016, **63**(1): 512-6.
[5] YIN Y, HE W, ZHANG L, *et al*. Preliminary design and optimization of a G-band extended interaction oscillator based on a pseudo-spark-sourced electron beam [J]. *Physics of Plasmas*, 2015, **22**(7):
[6] SHU G X, YIN H, ZHANG L, *et al*. Demonstration of a Planar W-Band, kW-Level Extended Interaction Oscillator Based on a Pseudospark-Sourced Sheet Electron Beam [J]. *IEEE Electron Device Letters*, 2018, **39**(3): 432-5.
[7] HE W, ZHANG L, BOWES D, *et al*. Generation of broadband terahertz radiation using a backward wave oscillator and pseudospark-

sourced electron beam [J]. *Appl Phys Lett*, 2015, **107**(13):
[8] CHEN H T, KERSTING R, CHO G C. Terahertz imaging with nanometer resolution [J]. *Appl Phys Lett*, 2003, **83**(15): 3009-11.
[9] CHERNIN D, BURKE A, CHERNYAVSKIY I, *et al*. 12.3: Extended Interaction Klystrons for terahertz power amplifiers; proceedings of the In Proc IEEE International Vacuum Electronics Conference, F, 2010 [C].
[10] CHANG Z, MENG L, YIN Y, *et al*. Circuit Design of a Compact 5-kV W-Band Extended Interaction Klystron [J]. *IEEE* Trans Electron Devices, 2018, **65**(3): 1179-84.
[11] XU C, MENG L, HU C F, *et al*. Analysis of Dual-Frequency Radiation From a G-Band Extended Interaction Oscillator With Double Sheet Beam [J]. *IEEE* Trans Electron Devices, 2019, **66**(7): 3184-9.
[12] BERRY D, DENG H, DOBBS R, *et al*. Practical Aspects of EIK Technology [J]. *IEEE* Trans Electron Devices, 2014, **61**(6): 1830-5.
[13] Extended Interaction Klystrons, Communications & Power Industries. Georgetown, *Ontario*, Canada, Oct. 31, 2001. [Online]. Available: https://www.cpii.com/product.cfm/4/40/156.
[14] BI L J, MENG L, YIN Y, *et al*. Design and Analysis of a High-Order Mode Ladder-Type RF Circuit for Stable Operation in a W-Band Extended Interaction Oscillator [J]. *IEEE* Trans Electron Devices, 2019, **66**(1): 729-35.
[15] CST Microwave Studio, CST, Darmstadt, Germany, 2014.
[16] JOYE C D, KIMURA T, HYTTINEN M, *et al*. Demonstration of a High Power, Wideband 220-GHz Traveling Wave Amplifier Fabricated by UV-LIGA [J]. *IEEE* Trans Electron Devices, 2014, **61**(6): 1672-8.
[17] GAMZINA D, HIMES L G, BARCHFELD R, *et al*. Nano-CNC Machining of Sub-THz Vacuum Electron Devices [J]. *IEEE* Trans Electron Devices, 2016, **63**(10): 4067-73.
[18] BURT G, ZHANG L, CONSTABLE D A, *et al*. A Millimeter-Wave Klystron Upconverter With a Higher Order Mode Output Cavity [J]. *IEEE* Trans Electron Devices, 2017, **64**(9): 3857-62.
[19] PAOLONI C. Periodically Allocated Reentrant Cavity Klystron [J]. *IEEE* Trans Electron Devices, 2014, **61**(6): 1687-91.
[20] XU C, WANG B, PENG R B, *et al*. Start current study of a THz sheet beam extended interaction oscillator [J]. *Physics of Plasmas*, 2018, **25**(7): 3103.
[21] ZHANG K, WU Z, LIU S. Study of An Extended Interaction Oscillator with A Rectangular Reentrance Coupled-cavity in Terahertz Region [J]. *Journal of Infrared*, Millimeter, and Terahertz Waves, 2009, **30**(4): 309-18.
[22] YIN Y, WANG B, LI H, *et al*. Study of the relation between the surface loss and the field flatness in the EID [J]. *International Journal of Electronics*, 2016, **104**(2): 204-17.
[23] DATTA S, KUMAR L, BASU B N. A Simple and Accurate Analysis of Conductivity Loss in Millimeter-Wave Helical Slow-Wave Structures [J]. *Journal of infrared*, millimeter and terahertz waves, 2009, **30**:381-92.